4 Search for $K\pi$-Atoms

Y. Allkofer, C. Amsler, S. Horikawa, I. Johnson[3], H. Pruys[4], C. Regenfus, and J. Rochet

In collaboration with:
Academy of Sciences of the Czech Republic, CERN, KEK (Tsukuba), Institute of Atomic Physics (Bucarest), JINR (Dubna), Laboratory Nazionali di Frascati, IHEP (Protvino), University of Basel, Bern, Ioannina, Kyoto, Lomonosov, Prague, Santiago, Trieste, Tokyo (Metropolitan) (DIRAC II Collaboration)

4.1 The $K\pi$ scattering length

The $K^-\pi^+$-atom is a hydrogen-like non-relativistic system of a K^- and a π^+ bound by the Coulomb force. Such atoms have not been observed so far, in contrast to $\pi^+\pi^-$ atoms which were observed and studied by the DIRAC Collaboration at CERN (1). For $K\pi$-atoms the binding energy of the 1s level is 2.9 keV and the Bohr radius 250 fm. The atom is unstable and decays into $\bar{K}^0\pi^0$ (Fig. 4.1). The atomic level is shifted by the overlap of the pion and kaon wave functions. The energy shift, determined by the scattering lengths a_1 and a_3 in the isospin 1/2 and 3/2 $K\pi$ states, respectively, is predicted to be about - 10 eV (i.e. towards stronger binding) (2). Up to a calculable small correction (2) the width Γ (or the lifetime τ) of the 1s level is related to the scattering lengths by the equation

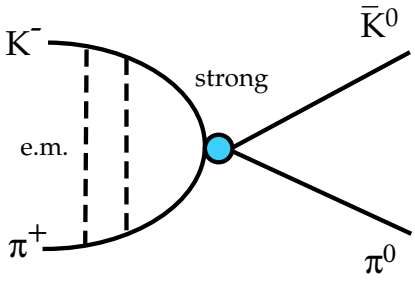

Figure 4.1: $K^-\pi^+$ **- atoms decay into** $\bar{K}^0\pi^0$**.**

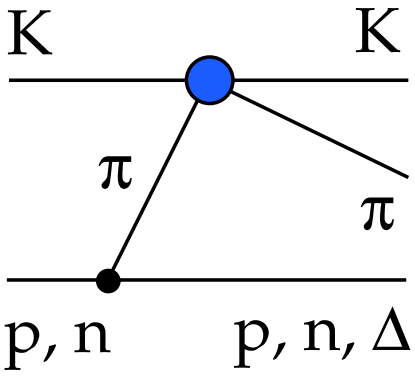

Figure 4.2: $K\pi$**-scattering in** Kp **- interactions.**

$$\Gamma = \frac{1}{\tau} = 8p^*\mu^2\alpha^3\left[\frac{a_1 - a_3}{3}\right]^2, \qquad (4.7)$$

where p^* = 11.5 MeV/c is the π^0 (or K^0) momentum in the rest frame of the atom, μ is the $K\pi$ reduced mass, and α the fine-structure constant.
Predictions for τ can, in principle, be derived from the $K\pi$ S - wave phase shifts obtained from $K\pi$ - scattering, e.g. by scattering kaons on nucleons (Fig. 4.2). We recall that the scattering lengths a_1 and a_3 are the *slopes* of the phase shifts $\delta_1(k)$ and $\delta_3(k)$ in the limit where the momentum k becomes vanishingly small. The scattering lengths a_1 and a_3 are poorly known. Figure 4.3 shows the S - wave $K\pi$ phase shifts from ref. (3). The δ_1 ($S_{1/2}$) - phase is poorly known below 1 GeV, showing a peculiar oscillation pattern. Above 1 GeV the S - wave interaction is dominated by the $K_0^*(1430)$ resonance. Figure 4.3 also shows the $P_{1/2}$ phase which is dominated by the $K^*(892)$ resonance. The interaction is attractive in the i = 1/2 and repulsive in the i = 3/2 state. The uncertainties in a_1 and a_3 are substantial: the extrapolation to zero energy from the various phase shift measurements disagree

[3]until October 2005
[4]until August 2005

by large factors: measurements of a_1 vary between 0.17 and 0.34 m_π^{-1}, those of a_3 between - 0.07 and - 0.14 m_π^{-1}. The scattering lengths were also computed from dispersion relations using scattering data, assuming analytical continuation, unitarity and crossing symmetry (4):

$$a_1 = 0.224 \pm 0.022\ \mathrm{m}_\pi^{-1} \text{ and}$$
$$a_3 = -0.0448 \pm 0.0077\ \mathrm{m}_\pi^{-1}. \qquad (4.8)$$

However, there are inconsistencies below 1 GeV/c (4). Using eqs. (4.7) and (4.8) one finds a mean life $\tau \sim 3.7$ fs for the $K\pi$ atom, with a rather large uncertainty.
The scattering lengths are of great importance for chiral perturbation theories (ChPT). The mean life of $\pi^+\pi^-$-atoms, recently measured by the DIRAC Collaboration (1), is in excellent agreement with predictions from ChPT (5) and with direct measurements of the scattering length from the $K \to \pi^+\pi^- e\nu$ decay (6). In contrast, the $K\pi$ - scattering length probes ChPT extended to s-quarks, i.e. in the limit where the masses of the u-, d- and s-quarks vanish. Figure 4.4 shows the prediction for a_3 vs. a_1 from ChPT predictions (7), together with the dispersion calculation from ref. (4). They are not in good agreement and there is a strong correlation between a_3 and a_1. The blue band shows the sensitivity of a hypothetical 20% accurate measurement of the lifetime of $K\pi$-atoms. A 20% measurement error in the lifetime leads to a 10% error in $|a_1 - a_3|$.

A measurement of the scattering length also yields information on nearby broad resonances. As mentioned above, S - wave $K\pi$ scattering is dominated by the $K_0^*(1430)$ resonance. However, there is mounting evidence for a very broad resonance around 800 MeV, the $K_0^*(800)$ (or κ). For example, recent data in $J/\psi \to K^+K^-\pi^+\pi^-$ report the κ at a mass of $\sim$ 800 MeV with a width of $\sim$ 600 MeV (8). Establishing the κ is essential to understand the nature of scalar mesons. The ground state nonet could be made of the four-quark states and/or meson-meson resonances $a_0(980)$, $f_0(980)$, $f_0(600)$ (σ) and $K_0^*(800)$ (κ) (9). If the latter indeed exists as a very broad state, it will influence the value of a_1.

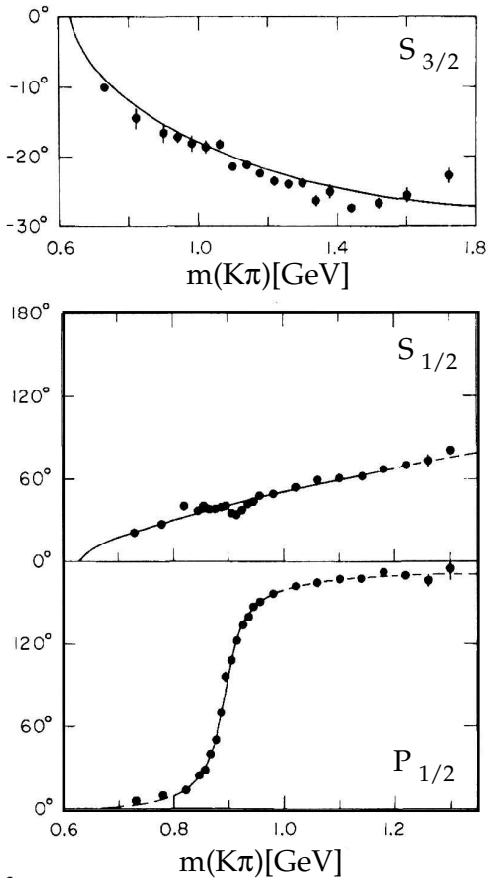

Figure 4.3: $K\pi$ phase shifts from ref. [3] showing the δ_3 ($S_{3/2}$), the δ_1 ($S_{1/2}$), and the $P_{1/2}$ phases as a function of $K\pi$ mass.

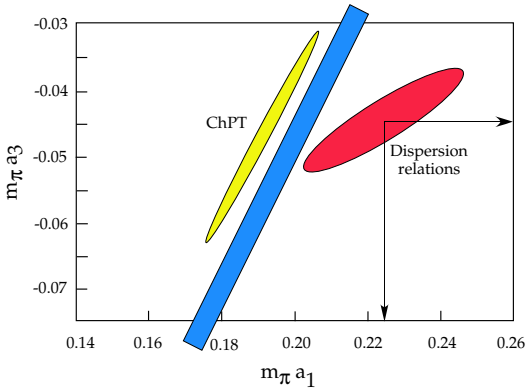

Figure 4.4: a_3 vs. a_1 from ChPT [7] and from dispersion relations [4]. The most recent measurements ($m_\pi a_1$ = 0.335 $\pm$ 0.006, $m_\pi a_3$ = - 0.14 $\pm$ 0.007, see ref. [3]) lie outside the range of this plot. The blue band shows the sensitivity of a 20% measurement of the mean life of $K\pi$-atoms.

4.2 The DIRAC II experiment

The Zurich group has joined the DIRAC experiment and will concentrate on the search and study of $K\pi$ - atoms. We will provide the aerogel Čerenkov counters for kaon detection and also the heavy gas system for the pion Čerenkov counters.

In the DIRAC apparatus kaons and pions are produced by the primary 24 GeV/c proton beam from the PS impinging on a 100 μm thick nickel foil (10). The emerging particles are analyzed in a double-arm magnetic spectrometer measuring the momentum vectors of two oppositely charged hadrons (Fig. 4.5). $K^-\pi^+$ - atoms, once produced, move forward and either annihilate into $\bar{K}^0\pi^0$ or ionize in the target. Since annihilation and ionization are competing processes, the mean life is obtained by measuring the breakup probability in the target, which can be calculated as a function of mean life. It is about 30 % in a 100 μm Ni target, assuming a mean life of 4.7 fs (11).

The breakup probability is given by the ratio of the number of dissociated pairs to the number of produced atoms. The dissociated kaon and pion emerge behind the target with a very small relative momentum $Q < 3$ MeV/c. One therefore expects an accumulation of events near $Q = 0$ which gives the number of dissociated pairs. Then one calculates the number of produced $K\pi$-atoms by measuring the number of unbound Coulomb pairs from the measured Q-distribution at large Q. The number of produced $K\pi$-atoms is obtained through a known relation between unbound and bound Coulomb pairs. This procedure has been applied to $\pi^+\pi^-$ atoms and details can be found in ref. (1).

The DIRAC apparatus (Fig. 4.5) has to be modified to discriminate between pions and kaons. Muons are identified by counters behind the concrete absorber. Electrons trigger the N_2 gas

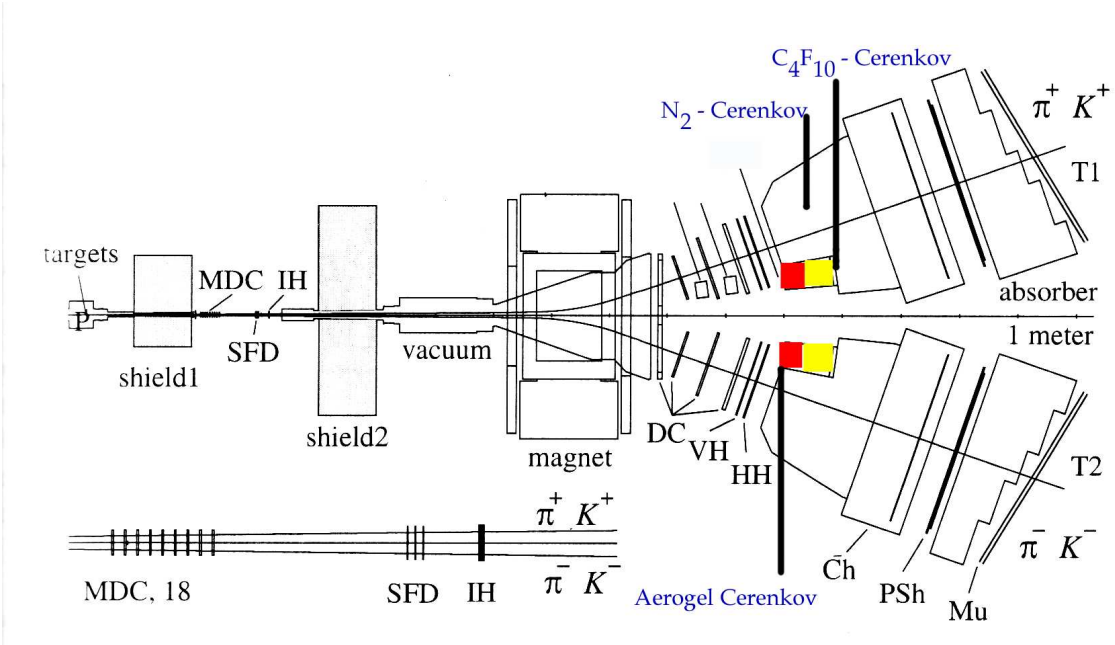

Figure 4.5: Sketch of the updated DIRAC spectrometer, showing the locations of the Čerenkov counters to identify electrons, pions and kaons. MDC = microdrift chambers, SFD = scintillating fibre detector, IH = ionization hodoscope, DC = drift chambers, VH, HH = scintillation hodoscopes, PSh = preshower, Mu = muon counters.

Čerenkov counter. The new C_4F_{10} gas Čerenkov counter identifies pions, while kaons are detected in the aerogel Čerenkov. Contaminating protons in the left arm are suppressed since they are below threshold for Čerenkov radiation. The right arm aerogel (for $K^-\pi^+$ - atoms) is not essential since the flux of antiprotons is much smaller than the flux of negative kaons.

4.3 The aerogel counters

Figure 4.6 shows the momentum distribution of kaons from $K\pi$-atoms at the entrance of the Čerenkov counters as a function of horizontal coordinate (in the plane of Fig. 4.5). This distribution was calculated using the known production cross sections at 24 GeV/c. Kaons from $K\pi$-atoms have momenta between 3.9 and 8.9 GeV/c. Figure 4.7 shows the vertical distribution which is not flat due to the slight upwards inclination of the spectrometers. For the emission of Čerenkov radiation the refractive index n has to be chosen so that $n > 1/\beta$ (where β is the velocity of the particle). Hence the quantity $n - 1$ has to be small enough to avoid signals from fast protons ($\beta \simeq 1$), yet large enough to detect kaons. In the momentum range covered by the apparatus, n is required to be typically 1.010, which is larger than can be achieved with pressurized gas counters and smaller than for all known solid or liquid radiators, except aerogel. One concludes from Fig. 4.6 and 4.6 that the aerogel counter has to cover a surface of about 35 x 40 cm^2.

Aerogel is made of colloidal SiO_2 grains of size $\sim$ 2 nm and pores $\sim$ 50 nm. The index of refraction depends on density ρ ($n = 1 + 0.21\rho$ [g/cm^3]). For example, for the $n = 1.008$ aerogel needed here, the density is 0.039 g/cm^3. The light yield is proportional to the factor

$$f = 1 - \frac{1}{\beta^2 n^2} \qquad (4.9)$$

which decreases quickly when $n \simeq 1$. This fact is the main difficulty with thin Čerenkov counters. As we show below in Fig. 4.9, a good $K-p$ separation can be achieved with two indices of refraction, n = 1.008 and 1.015. The lowest index is needed to improve the separation in the region of high energy protons close to the primary beam line.

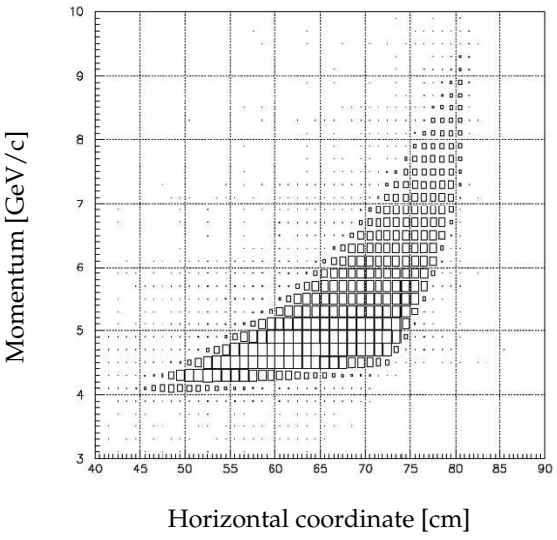

Figure 4.6: Momentum distribution of kaons from the breakup of $K\pi$-atoms. Small angles with respect to the primary proton beam are towards the right.

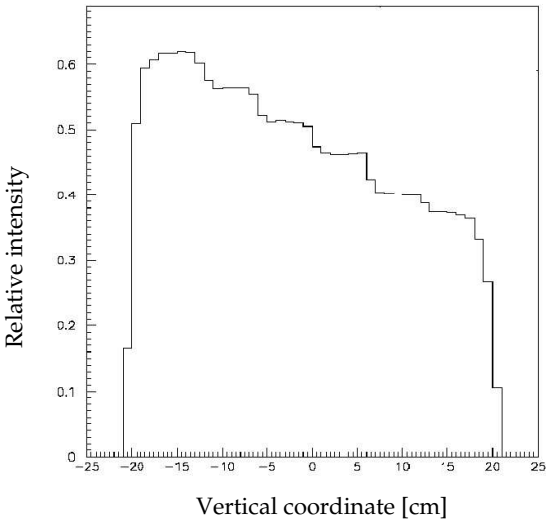

Figure 4.7: Vertical distribution.

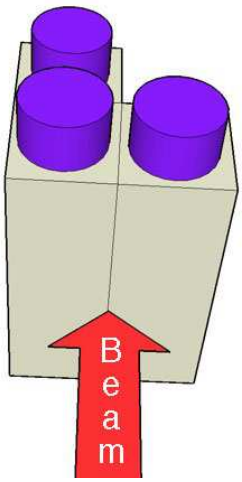

Figure 4.8: Three aerogel counters are needed to separate protons from kaons. The upstream pair has n = 1.015, the downstream counter n = 1.008. Small angles with respect to the primary proton beam are towards the left.

The 1.015 counter is segmented into two parts to reduce pileup. Figure 4.8 shows the conceptual design. Each counter is vertical (40 cm long) viewed by two photomultipliers, one at each end.

We have initiated an R&D program to measure the light yield of aerogel and to optimize the geometry. Most of the measurements were made with n = 1.05 aerogel which is easily available. We have measured the number of photoelectrons $N_{p.e.}$ for a thickness of 10 cm of aerogel and for a 10 cm long slab viewed by two photomultipliers (PM) with UV windows. The measurements were made with cosmic ray muons which have an average momentum of 700 MeV/c ($\bar{\beta}$ = 0.989) since test beams were not available at CERN in 2005. We have obtained about 3 photoelectrons / cm of aerogel (summing the signals from both tubes). Extrapolation from n = 1.05 to lower indices and β = 1 can then easily be made using eq. (4.9).

However, the absorption length increases rapidly from about 10 cm at 270 nm to 3 m at 350 nm (12). Therefore, 40 cm long aerogel counters are likely to be problematic. Figure 4.9 shows the expected average number of photoelectrons as a function of momentum for kaons and protons. The upper boundaries of the bands are for particles traversing the counter close to one of the PM, the lower boundary for those crossing the counter in the middle. The strong absorption can be compensated by increasing the thickness of aerogel in the middle of the counter (see Fig. 4.16 below), which is easily feasible since aerogel is delivered in 1cm thick tiles. Figure 4.10 shows a simulation of the signal attenuation.

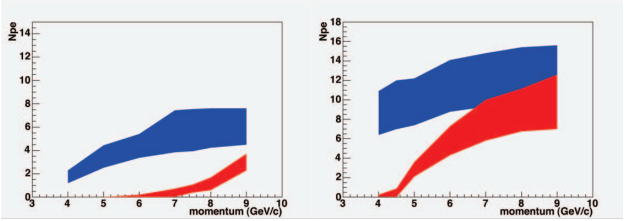

Figure 4.9: Average number of photoelectrons as a function of momentum for n = 1.008 (left) and 1.016 (right) for a thickness of 15 cm and a length of 40 cm.

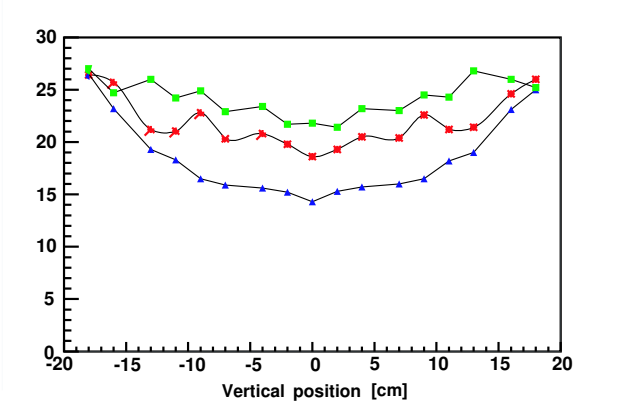

Figure 4.10: Signal amplitude as a function of the distance at which the particle crosses the aerogel counter (arbitrary scale). The photomultipliers are located at the edges ($\pm$ 20 cm). The blue (bottom) curve is for a counter with constant thickness, the red (middle) curve for 4 additional tiles and the green (top) curve for 6 additional tiles in the middle of the counter.

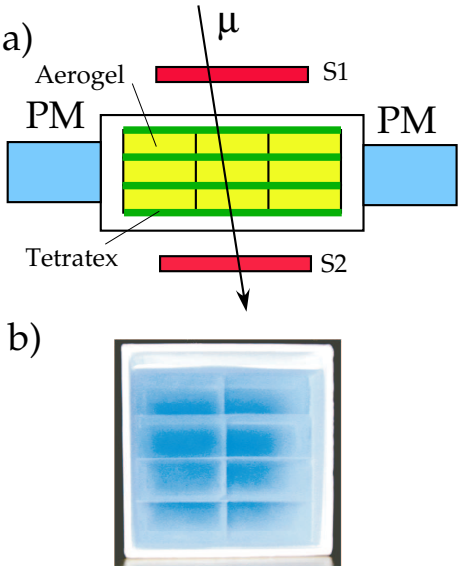

Figure 4.11: a) setup for light yield measurements,
b) photograph of the aerogel tiles.

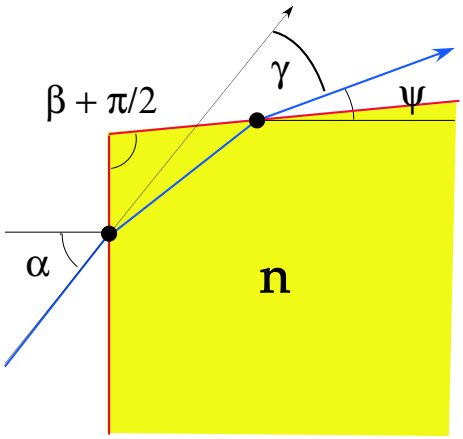

Figure 4.12: Principle of setup to measure the refractive index.

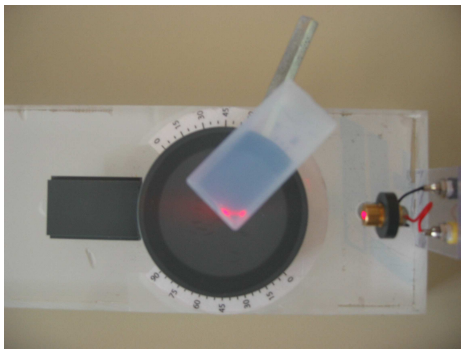

Figure 4.13:Photograph of the setup.

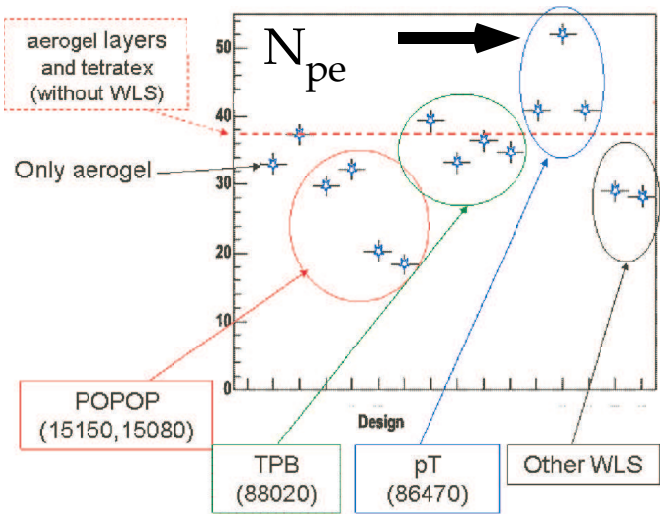

Figure 4.14:
Number of photoelectrons for a 10 cm thick, 10 cm long, n=1.05 aerogel counter, using cosmic muons, and for different geometries and WLS. The arrow shows the optimum design with p-terphenyl dissolved in chloroform.

We also tried a novel setup using wavelength shifters (WLS). Figure 4.11 shows the arrangement in our lab. The 2.5 cm thick aerogel tiles were sandwiched between reflective Tetratex foils which were sprayed with WLS. For example, p-terphenyl dissolved in chloroform shifts light from 270 to 340 nm, which reduces absorption and leads to some 5.5 p.e. /cm or 7 p.e. /cm for $\beta = 1$ (Fig. 4.14). Using this last figure one then expects about 3 (12) photoelectrons at 4.5 (8) GeV/c for 15 cm of 1.008 aerogel. These results are quite encouraging when compared to Fig. 4.9a, but they need to be checked with a prototype of the final length and depth.
We have also built a simple apparatus to measure the refractive index of aerogel using the refraction of a laser beam, following ref. (12). Figures 4.12 and 4.13 show a tile of aerogel illuminated by a laser beam incident under the angle α. One measures the displacement of the beam spot on a distant screen, i.e. the deflection γ of the beam which exits the aerogel:

$$\gamma = \alpha - \beta + \frac{\pi}{2} + \mathrm{asin}[\sin\alpha \sin\beta + n\sqrt{1 - \frac{\sin^2\alpha}{n^2}} \cos\beta]. \quad (4.10)$$

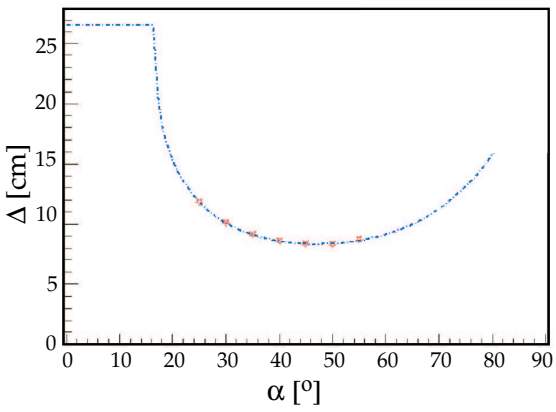

Figure 4.15:
Measurement of laser spot displacement as a function of incident angle, with fit following eq. (4.10).

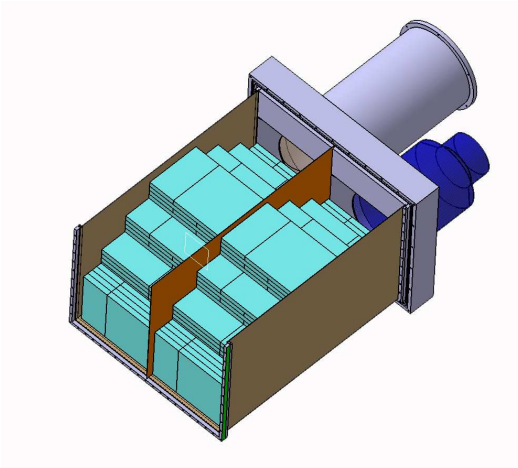

Figure 4.16:
Exploded view of the n = 1.015 aerogel counter showing the pyramidal design.

With at least two incident angles α one can eliminate β (expected to be around 0^0). Figure 4.15 shows the measurements for a piece of n = 1.05 aerogel, together with the fit leading to $n = 1.055 \pm 0.002$.

Figure 4.16 shows the design of the n = 1.015 aerogel detector built in the workshop of the Physik - Institut. The 5" Photonis - Philips XP4570/B photomultipliers with UV windows will be used. The 14 ℓ of n = 1.008 aerogel has been produced by the Budker and Boreskov Institutes in Novosibirsk, the 24 ℓ of n = 1.015 by Panasonic. The construction and tests are being performed in early 2006 and the detectors will be installed in the summer of 2006, when DIRAC resumes data taking. DIRAC (PS212) has been approved by the CERN Research Board to run at least until 2008. Extrapolating from $\pi\pi$ data, we estimate that some 1000 $K\pi$-atoms should be observed by DIRAC during 2006 - 2008.

[1] B. Adeva *et al.* (DIRAC Collaboration), Phys. Lett. **B 619** (2005) 50.
[2] J. Schweizer, Eur. Phys. J **C 36** (2004) 483; Phys. Lett. **B 587** (2004) 33.
[3] P. Estabrooks *et al.*, Nucl. Phys. **B 133** (1978) 490.
[4] P. Büttiker, S. Descotes-Genon, B. Moussallam, Eur. Phys. J. **C 33** (2004) 409.
[5] G. Colangelo, J. Gasser and H. Leutwyler, Nucl. Phys. **B 603** (2001) 125 and references therein.
[6] S. Pislak *et al.*, Phys. Rev. **D 67** (2003) 072004.
[7] V. Bernard *et al.*, Nucl. Phys. **B 357** (1991) 129.
[8] M. Ablikim et *et al.* (BES Collaboration), Phys. Lett. **B 633** (2006) 681.
[9] For a review see C. Amsler and N. Törnqvist, Phys. Rep. **389** (2004) 61.
[10] B. Adeva *et al.*, Nucl. Instr. and Meth. in Phys. Research **A 515** (2003) 467.
[11] B. Adeva *et al.*, Add. to DIRAC proposal, CERN - SPSC - 2004 - 009.
[12] A. R. Buziatev *et al.*, Nucl. Instr. Meth. in Phys. Research **A 433** (1999) 396.